Building a Pulse Detector using the Frequency Resolved Optical Gating Technique

J. Vallin

Stanford Linear Accelerator Center, Stanford University, Stanford, CA 94309

Building a Pulse Detector using the Frequency Resolved Optical Gating Technique

Jose Vallin

Office of Science, ERULF Program

San Jose State University

SLAC

Menlo Park, CA

15 August, 2002

Table of Contents

Table of Contents Continues

Tables

Abstract

We show how to construct a diagnostic optical layout known as Frequency Resolved Optical Gating (FROG) for an ir mode-locked laser by using the nonlinear effect known as second harmonic generation (SHG). In this paper, we explain the principle of operation and the theory upon which this diagnostic is based. Moreover, we described the procedure used to measure the duration and frequency components of a pulse. This process consists of calibrating the scales of a two-dimensional image, time delay vs. frequency, known as FROG spectrogram or FROG trace. This calibration of the time delay scale yields the correspondence between a pixel and time delay. Similarly, the calibration of the frequency scale yields the correspondence between a pixel, and frequency.

Introduction

In research, diagnostic development is a must. Diagnostics validate the performance of breakthrough technology, which is used in the laboratory by researchers doing modern and innovative research. If scientists were not able to corroborate the performance of the technology used to carry out their experiments, then their research would not be credible. The cornerstone of science is based upon the notion of substantiating and reproducing results. Thus, diagnostic development is an important pillar on which scientific research is based. Once new technology is developed, it may be implemented in research to yield new insight into our current knowledge. Moreover, diagnostics afford a means for optimizing technology. An excellent example is the development of the laser in the late 1950's. Once the properties of the laser such as monochromaticity, intensity, and directionality were properly diagnosed, improvements over the prototype were made. The progress in laser technology has made the laser an indispensable tool in the advancement of scientific research and technology. Thus, diagnostics not only serve to analyze performance, but it also yield ideas essential for optimization.

There are two types of laser: continuous wave form (CW) and pulse lasers. Of these two types, ultrashort pulse lasers have "increasingly meet the stringent specifications and reliability necessary for many industrial and medical applications such as telecommunication, imaging, and laser eye surgery" (Hopkins, Sibbett, 2000). Currently, the broadband multimedia industry is looking into using broadband low-power infrared lasers to transmit broadband signals from the optical-fiber backbone to many end users and back (Acampora, 2002).

We can currently produce mode-locked laser oscillators that operate with thousands of longitudinal modes. Because we have the technical capability to generate laser pulses that are the sum of thousands of longitudinal modes, which are locked in phase, we therefore know that such laser output will be in the form of pulses of ultrashort duration. The duration of a pulse commonly refers to the Full Width at Half its Maximum value (FWHM), and the term ultrashort is reserved for a laser pulse that is less than a pico-second. Phenomena occurring in the ultrashort scale are therefore referred to as dynamically ultrafast (P. Bolton, personal interview, July 12, 2002). Each individual ultrashort laser pulse therefore Fourier transforms to a broad spectral bandwidth (Verdeyen, 1995, p, 296). Thus, the terms ultrashort, ultrafast, and broadband refer to the same concept: a pulse of short duration. According to Paul Bolton, the ability to monitor ultrafast behavior is therefore necessary not only with respect to the output of the mode lock oscillator output but also with respect to any ultrafast phenomena induced by such fast pulses.

This project entailed the development of a diagnostic for an infra-red laser pulse. The current technology of choice is frequency resolved optical gating (FROG) (Paul Bolton, personal communication, July 12, 2002), which is "a simple, intuitive, self-contained, and general technique that achieves the full measure [of the amplitude and phase history of the electric field of an ultrashort pulse]"(Kane, Trebino, 1993). Frequency resolution comes from time-resolving the spectral components of the ultrashort-pulse. The time dependent optical gating is associated with the interaction of two coincident pulses. The time and frequency two scales are orthogonal and must be

calibrated. This diagnostic produces a two-dimensional image, which we refer to as a
FROG spectrogram or FROG trace (see figure 1).
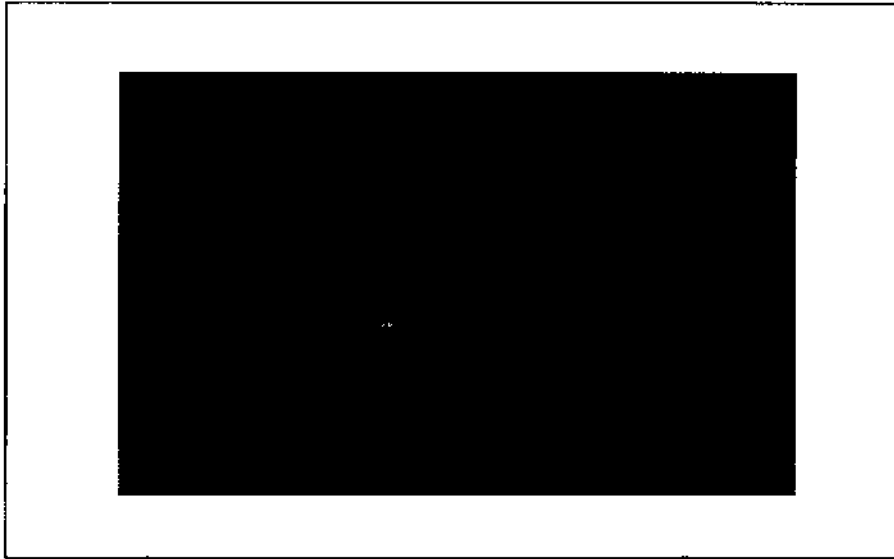
Figure 1. FROG trace

This provides a physically intuitive description of a single ultrashort laser pulse because
it contains the time dependence of the spectrum (Paul Bolton, personal communication,
July 12, 2002). The goal of the project was to generate and calibrate such two-
dimensional images with femtosecond resolution.

Choice of FROG

Daniel J. Kane and Rick Trebino first introduced the FROG technology in 1993
(Kane, Trebino, 1993). There are several geometries that use the FROG technique. We
have employed the second harmonic generation (SHG) form of this diagnostic, which is
appropriate for measuring low energy pulses that are in the nanojoule range (Kane,
Trebino, 1994). The SHG FROG has single shot capability.

It should be noted that the FROG spectrogram amounts to adding a frequency
dimension to what an "optical" oscilloscope would provide (P. Bolton, personal

communication, July 12, 2002). This capability to resolve the frequency of an ultrashort pulse is what makes the FROG technology diagnostic so advantageous and exciting.

The SHG FROG was built in several steps. First, a layout was assembled (see diagram 2). Then, this layout was aligned and calibrated using a CW infrared laser. Then, a mode-locked oscillator (MIRA), which produces a pulse train of sub-picosecond pulses separated by 13.1 nanoseconds (76.3 MHz), was propagated through the system. Time delay and frequency scales of an autocorrelated second harmonic (blue) beam were calibrated.
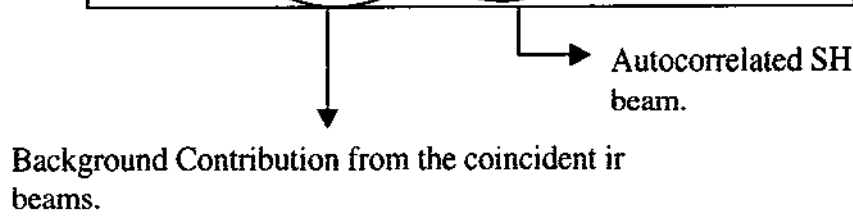
Principle of Operation

Before the invention of the FROG technology, direct measurement of the phase and intensity of an ultrashort pulse was not possible (Kane, Trebino, 1993). The only measurable characteristic of ultrashort pulses was its duration, and the technique used was autocorrelation or optical gating alone (Salin, Georges, Roger, and Brun, 1987). Autocorrelation consists of splitting an incident pulse into two comparable intensities

(1) $I_{tot} = I_f(t) - I_v(t - \Delta t_o)$

with a beam splitter and making the resulting pulses coincident at a point where a suitable crystal for SHG is placed (see diagram 1). If I_f and I_v are the intensities of the pulse that travels a fix and a variable path respectively, then the autocorrelated signal in the middle beam is known to be:

(2) $S(\Delta t_o) = A \cdot \int ((I_f(t'))^2 + (I_v(t'))^2 + 2 \cdot I_f(t') \cdot I_v(t' - \Delta t_o)) \, dt'$

Autocorrelated SH beam.

Background Contribution from the coincident ir beams.

The key to this technique is to control the optical path length of these two coincident pulses. If the intensities of the coincident pulses are high enough, a process known as SHG ensues. It will be shown later in this paper that a monochromatic optical field incident on a second order nonlinear crystal can radiate a second harmonic. The third term of equation (2) represents a pulse formed from the autocorrelation of the two coincident pulses. This second harmonic light field contains the autocorrelation information that we can measure. The first two background terms in equation (2) represent electromagnetic radiation, which complicates the interpretation of the autocorrelation data. By analyzing the response of the middle beam only to an induced time delay in one of the two pulses, the duration of the pulse can be measured. This is what is called Background-Free Autocorrelation by Non-Collinear Phase Matching (Operator's Manual ..., p. 7-25 – 7-26).

The FROG technique used here was built upon the autocorrelation technique by dispersing the middle second harmonic beam with a diffraction grating as shown in diagram 2.

Theory

To understand the origin of SHG one must start from Maxwell's equations. The origin of SHG can be seen by analyzing a system's response to an electromagnetic wave and by assuming that its response is nonlinear. Using Maxwell's equations, it can be shown that the source of the light scatter by nonlinear crystal is the induced nonlinear polarization on the crystal by the incident light. The electric field, **E**, of a laser pulse and the nonlinear polarization, $\mathbf{P_{NL}}$, are related according to:

(3) $\quad -\nabla^2 E + \dfrac{n^2}{c_o^2} \dfrac{\partial^2 E}{\partial t^2} \approx -\mu \cdot \dfrac{\partial^2 P_{NL}}{\partial t^2}$; { $S \equiv -\mu \cdot \dfrac{\partial^2 P_{NL}}{\partial t^2}$, source radiating in the med. }

(4) $\quad \therefore,$

$$\boxed{-\nabla^2 E + \dfrac{n^2}{c_o^2} \dfrac{\partial^2 E}{\partial t^2} \approx S}$$

— Wave equation of a nonlinear medium.
Note that the source of the scattered light is **S**.

where μ and n are the permeability and the index of refraction of the crystal respectively, and c_o is the speed of light in free space.

A medium whose induced polarization density is proportional to the square of the electric field is called a second-order nonlinear medium. The response of a second-order nonlinear medium to an electric field of an angular frequency ω and complex amplitude $E(\omega)$, $E(t) = E(\omega) \cdot \exp(j\omega t)$, can be analyzed by evaluating the expression of the nonlinear polarization.

(5) $\quad P_{NL}(t) = 2d \cdot E^2$

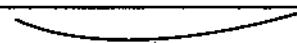$\quad\quad\quad = 2(\text{ Real}(E(\omega) \cdot \exp(j\omega t)))^2$, only the real part of the **E** is observable.

$P_{NL}(t) = 2d[\dfrac{E(\omega) \cdot \exp(j\omega t)+ E^*(\omega) \cdot \exp(-j\omega t)}{2}] \cdot [\dfrac{E(\omega) \cdot \exp(j\omega t) + E^*(\omega) \cdot \exp(-j\omega t)}{2}]$

$\quad\quad = \dfrac{2 \cdot d}{4} [E^2(\omega)\exp(j2\omega t) + E^{*2}(\omega)\exp(-j2\omega t) + 2E(\omega)E^*(\omega)]$

$\quad\quad = d \cdot E(\omega)E^*(\omega) + d \cdot [\dfrac{E^2(\omega)\exp(j2\omega t) + E^{*2}(\omega)\exp(-j2\omega t)}{2}]$

$\quad\quad = d \cdot E(\omega)E^*(\omega) + d \cdot [\text{ Real } (E^2(\omega) \cdot \exp(j2\omega t))]$; { $P_{NL}(0) = d \cdot E(\omega)E^*(\omega)$,

$\quad\quad\quad\quad\quad\quad\quad\quad\quad\quad\quad\quad\quad\quad\quad\quad\quad\quad\quad\quad P_{NL}(2\omega) = d \cdot E^2(\omega)$

(5)

$$\boxed{P_{NL}(t) = P_{NL}(0) + P_{NL}(2\omega) \cdot \text{Real}(\exp(j2\omega t))}$$

DC term $\quad\quad\quad\quad\quad\quad\quad\quad$ 2nd harmonic

Thus, a second-order nonlinear medium responds to a monochromatic wave of frequency ω by radiating a wave at frequency 2ω. This is referred to as SHG.

To obtain a SH beam, k_3, that is optimum, its wave vector must add up to the sum of the two coincident wave vectors. This is a statement of the phase matching condition and an expression of momentum conservation.

(6) $k_3 = k_f + k_v$.

This condition determines the efficiency (intensity) of the generation of k_3. Graphically, this condition can be pictured as follows:
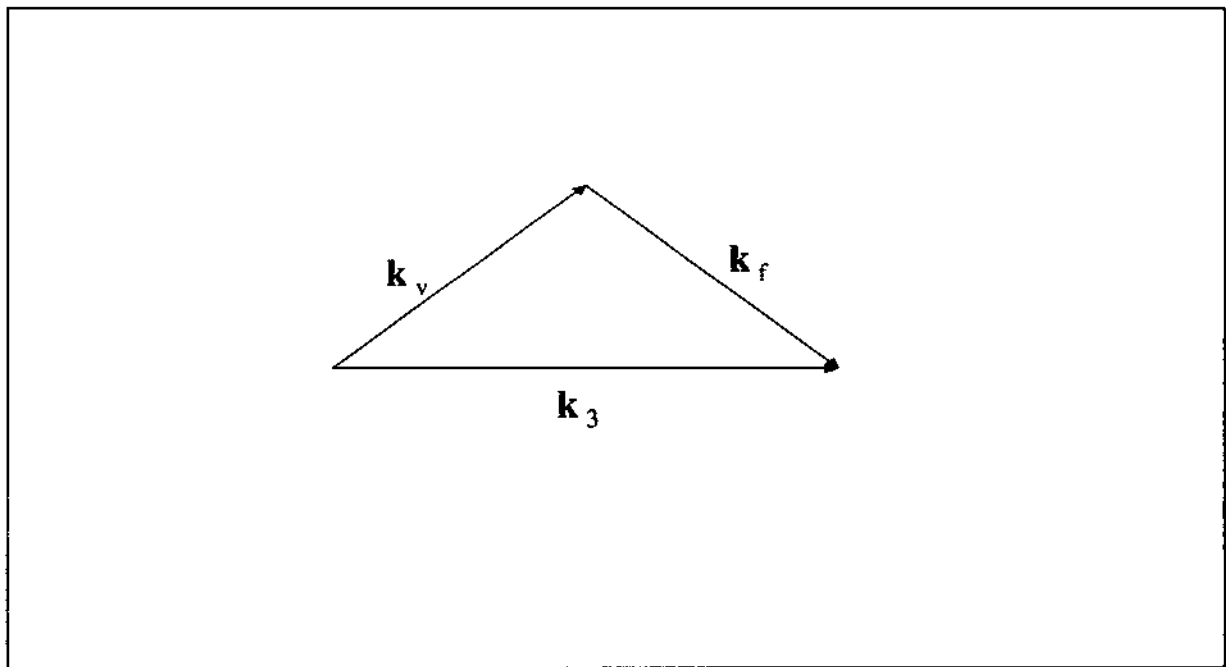
Figure 2. Noncollinear Phase Matching Condition

This form of SHG is a three wave mixing process. In this process, which is the degenerate case, two photons of ir-wavelength (756 nm) mix to produce a photon of blue wavelength (378 nm) and vice versa (i.e., one photon of blue wavelength decays into two

photons of ir-wavelength). This happens simultaneously in the course of propagation through the crystal. This process is optimized when the ir and blue electromagnetic waves propagate together through the crystal. Therefore, ir and blue electromagnetic beams propagate at the same speed. This optimization condition leads to a glaring paradox: how can two waves of two different frequencies propagate at the same speed in the same medium? This paradox is solved by the anisotropy of the crystal.

An anisotropic crystal's index of refraction experienced by an electromagnetic wave propagating through it depends in the direction of propagation. This implies that the constitutive relations

$$(7) \quad \mathbf{D} = \in \mathbf{E} \quad \text{and} \quad (8) \quad \mathbf{P} = \in \mathbf{E} \; ; \; \in \; \equiv \in_o (1 + \chi_e)$$

$\downarrow$

Electric Susceptibility

are no longer isotropic in addition to being nonlinear. To account for this anisotropic effect, the electric susceptibility must be a three by three matrix that characterizes the dielectric properties of the crystal. For symmetric crystals (i.e., crystals characterized by six degrees of freedom), a coordinate system can always be found for which off-diagonal elements vanish. Figure 2 below represents the geometrical representation of a symmetric, negative (i.e., $n_e < n_o$), uniaxial (i.e., $n_1 = n_2 = n_o$) crystal, where k_3 represents the directions of the SHG signal that we need to optimize.
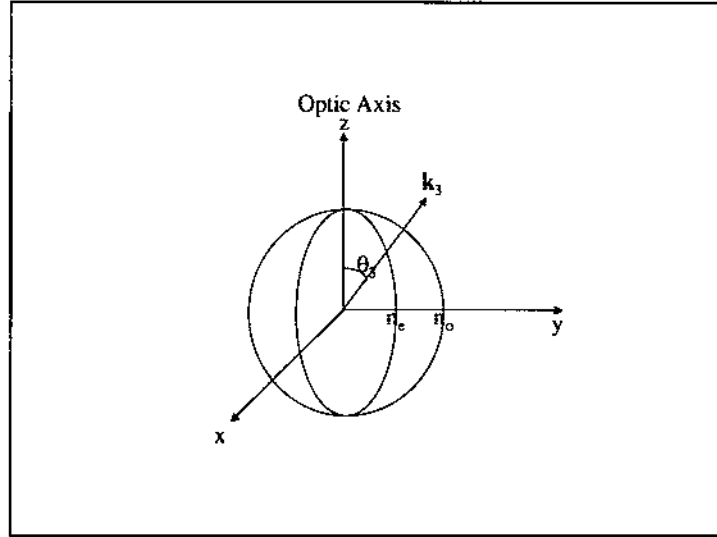
Figure 3. Geometrical representation of a negative uniaxial crystal

The index of refraction experienced by k_3 depends on the angle θ, which is defined with respect to the optic axis. The circle represents the uniform index of refraction n_o. This figure clearly shows that $n_o(\omega) \neq n_\theta(\omega)$ for $\theta \neq 0$. However, we can make $n_o(\omega) = n_{\theta 3}(2 \cdot \omega)$. This is what is called Type I phase matching. The efficiency of the Second Harmonic in the k_3 direction is determined by the extent to which Type I phase matching is satisfied.

It should be noted that to determine θ_3 the optic axis orientation of the crystal must be known. This optic axis is given in the datasheet of the crystal, and its orientation can be specified at the time of purchased from the manufacturer. In this project, a BBO crystal whose optic axis orientation was unknown was used. Yet, we were able to confirm experimentally within angular measurement error of $| 1° |$, that our geometry was consisten with Type I phase matching.

Data Analysis

In the laboratory, we measured the angle between the two incident pulses to be

23° (see figure 4). Thus, we can use the wave vectors of the coincident pulses and

autocorrelated SHG beam to construct a vectorial representation of momentum

conservation – equation (14) (see figure 5).
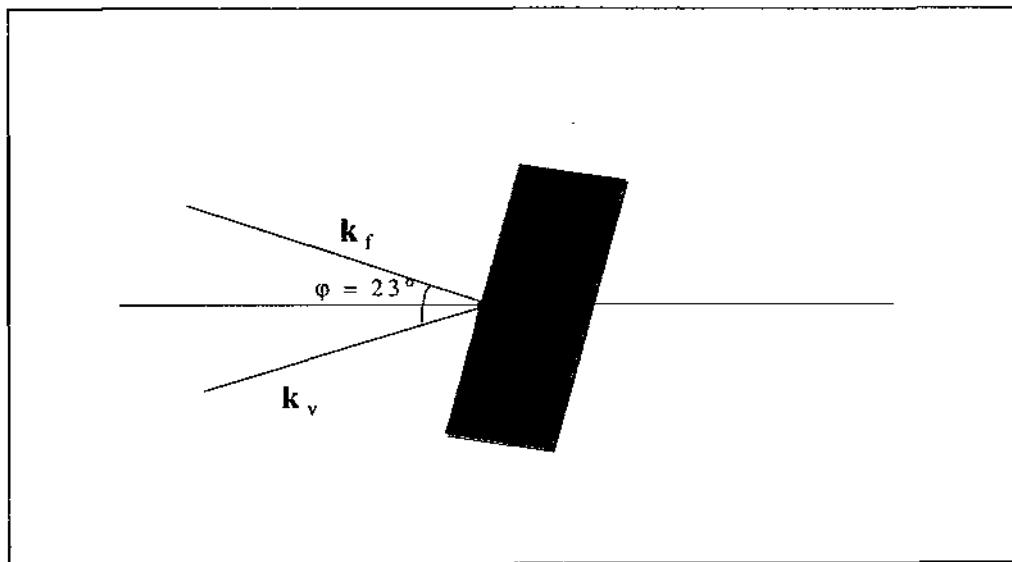
Figure 4. Diagram of Coincident Pulses
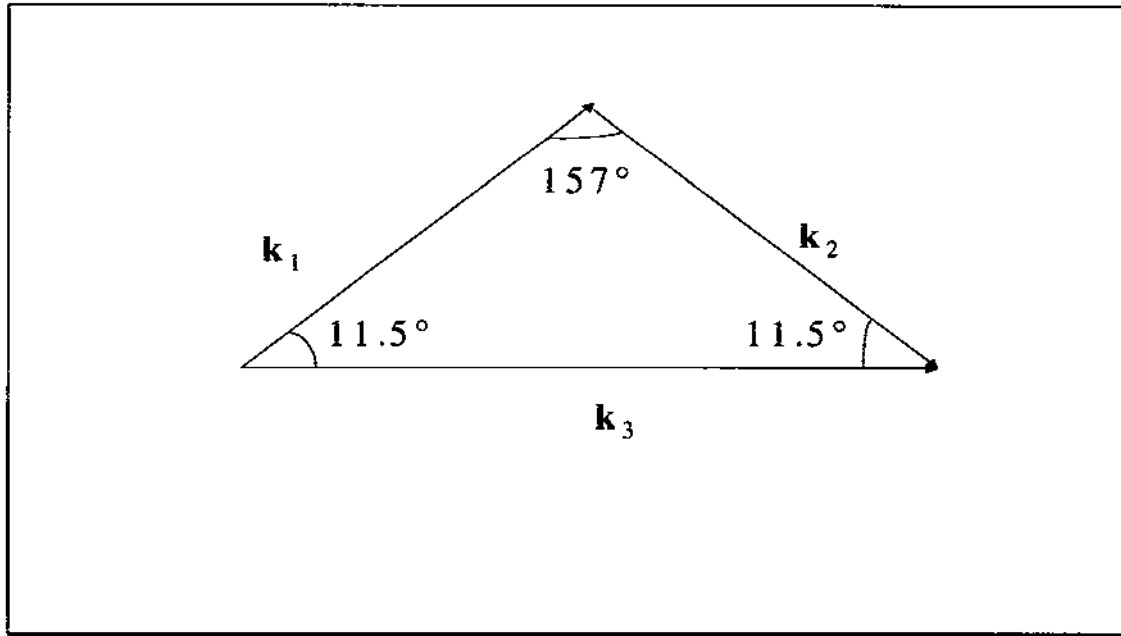
Figure 5. Momentum Conservation Geometry

Knowing the angles of this isosceles triangle allowed us to determine the non-collinear phase matching condition. Since we know that

(9) $|\mathbf{k_1}| = |\mathbf{k_2}| = \dfrac{2\pi n_O(\omega)}{\lambda_o}$;

(10) $|\mathbf{k_3}| = \dfrac{2\pi n_\theta(2\omega)}{\lambda_3}$

(11) $\lambda_3 = \dfrac{\lambda_o}{2}$

We can determine $n_\theta(2\omega)$ in terms of $n_1(\omega)$ by invoking the Law of Sines in the isosceles triangle of Figure 4 to be:

(12) $\Rightarrow$ $\boxed{n_\theta(2\omega) = .98 \cdot n_1(\omega)}$

11

If we assume an experimental angular measurement error of plus or minus 1°, then the percent error difference is plus or minus .04. Thus, $n_\theta(2\omega) = (.98 \pm .04) n_1(\omega)$, which is consistent with Type I Phase Matching as expected.

The FROG optic layout consisted of two broadband concave mirrors (M9, M8) of 99.8 percent reflectivity and 50 centimeter radius of curvature. These mirrors focused the two coincident pulses onto a Beta Barium Borate (BBO) crystal of unknown optic axis orientation. Five broadband flat mirrors coated for 756 nanometer wavelength and optimized for 45 degree incidence (M1, M2, M3, M4, M5, M6) were used to steer the two coincident pulses to the two concave mirrors. A Thermo Jarrell Ash, interferometrically ruled reflection grating with 1,200 grooves per millimeter and optimized (blazed) for 400 nanometer wavelength was used to disperse autocorrelated signal that yielded the FROG Spectrogram. A 50 % beam splitter (BS) coated for 756 nanometer wavelength and optimized for 45 degree incidence completes the list of optical components used in the FROG layout. The optics were purchased from CVI Laser.

The laser diagnosed with this FROG optical layout was a 900 MIRA infra red titanium:saphire modelocked laser pumped by a 530 nanometer, MILLENNIA (S/N 1152), Spectra-Physics Laser. A Vector S310, SCIENTECH power meter, measured the average power of the pulse train to be typically 365 mW (see diagram 3). A Tektronix 2467, 350 MHz oscilloscope, measured the pulse separation between two consecutive pulses to be 13.1 nanoseconds. The repetition rate of the mode-locked train was therefore 76.3 MHz.

To calibrate the time delay scale of the FROG trace, the optimum setting for generation of the autocorrelated blue beam was estimated. This setting was defined to

have a time delay of zero, $\Delta t_o = 0$. Then, an incremental time delay was introduced

above and below the optimum time delay, which causes the FROG trace profile to

laterally shift in one direction when viewed on the monitor. By capturing the image of

the FROG trace at every time delay setting with a HITACHI KP-160 CCD camera and

ImageGrabber 2.1 software, I obtained the time profile of every setting with NIH Image

1.54 software and determined the FWHM and the pixel value of the peak of these profiles

(see table 1). In each case, this was integrated over the full spectrum. By measuring the

shift of the time profile (in pixels) with respect to the optimum setting, Δp (see table 2),

the correspondence between a pixel and time was calculated. This is possible because Δp

is related to the induced time delay, Δt_o, by

(13) $\quad \Delta x_o = \dfrac{c\Delta t_o}{2n\sin(\varphi/2)} \quad ; \quad$ { $\varphi \equiv$ angle of coincident pulses
$\qquad\qquad\qquad\qquad\qquad\quad = 11.5°$, measured.

$$n = \frac{n_o + n_e}{2} = \frac{1.6673 + 1.550}{2} = 1.60865$$

$$c = \text{speed of light}$$
$$= 2.998 \times 10^8 \text{m/s}$$

where n is the index of refraction of the BBO crystal used this project. By relating Δp to

Δx_o,

(14) $\Delta p \equiv \dfrac{\Delta x_o}{\alpha}$

we were able to calculate the shift of every profile, Δp, with respect to a corresponding

time delay Δt_o in terms of α.

$\Rightarrow \qquad \Delta p = \dfrac{c\Delta t_o}{2 \cdot n \cdot \alpha \cdot \sin(\varphi/2)}$

$\Rightarrow \qquad \dfrac{\Delta p}{\Delta t_o} = \dfrac{(2.998 \times 10^8 \text{m/s})}{2 \cdot 1.60865 \cdot \sin(23°/2)} \, \Delta t_o$

$$(15) \quad \boxed{\frac{\Delta p}{\Delta t_o} = \frac{4.67 \times 10^8}{\alpha}}$$

From the plot Δp vs. Δt_o (see graph 1), one can conclude that a pixel per second equals

9.95×10^{13} (i.e., $\Delta p/fs = .0995$). Thus, from equation (15)

$$\frac{\Delta p}{\Delta t_o} = \frac{c\Delta t_o}{2 \cdot \alpha \cdot n \cdot \sin(\varphi/2)} . = 9.95 \times 10^{13} \text{ pixels/sec.}$$

$$\Rightarrow \quad \alpha = \frac{c\Delta t_o}{(\frac{\Delta p}{\Delta t_o}) \cdot 2 \cdot n \cdot \sin(\varphi/2)} .$$

$$\Rightarrow \quad \alpha = \frac{2.998 \times 10^8 \text{ m/s}}{9.95 \times 10^{13} \text{ pixel/s} \cdot 2 \cdot 1.60865 \cdot \sin(23°/2)} .$$

$$(16) \quad \Rightarrow \quad \boxed{\alpha = 4.69 \times 10^{-6} \text{ m/pixel}}$$

Thus, if $\Delta p = 1$ pixel, then $\Delta t_o = \frac{\alpha \cdot 2 \cdot n \cdot \sin(\varphi/2)}{c}$

$$\Delta t_o = \frac{2 \cdot 9.69 \times 10^{-6} \text{ m} \cdot 1.60865 \cdot \sin(23°/2)}{2.998 \times 10^8 \text{ m/s}}$$

$$(17) \quad \boxed{\Delta t_o = 10.0 \times 10^{-15} \text{ s} = 10 \text{ femtoseconds}}$$

Since $\Delta x_o \equiv \alpha \Delta p$, a pixel value difference of the peak of every profile with respect to the

optimum setting of 1 corresponds to a profile shift of 4.69 μm ($\alpha = 4.69 \times 10^{-6}$ m/pixel $\cdot$ 1

pixel $= \Delta x_o$) and a time delay of ten femtoseconds. Since the average FWHM of every

profile analyzed was measured to be 200.2 pixels, the duration of the pulse turns out to be

(200.2pixels)$\bullet$ (10.0 femtoseconds / pixel) = 2002 femtoseconds. This result is incorrect

however because the equation used to relate the induced time delay, Δt_o, and the profile

shift, Δx_o, assumes collimated coincident pulses, and therefore, a collimated

autocorrelation blue beam. Since we are calibrating the "divergent" autocorrelated beam case, a temporal enhancement factor, Λ, needs to be determined for pulsewidth increments.

To calibrate the frequency scale, we made use of a S2000 Fiber Optics Spectrometer to obtain an independent measurement of the infrared pulse being diagnosed (see diagram 4). The Fiber Optics Spectrometer was used to measure the spectral bandwidth of the infrared pulse at the optimum setting. An image of the FROG trace was captured at this setting. Then, a 2 nanometer change in the ir wavelength was induced. The Fiber Optics Spectrometer was used again to measure the spectral bandwidth of this new ir pulse. An image of the FROG trace corresponding to this new pulse was also taken. Since a two nanometer change in wavelength in the ir pulse corresponds to a one nanometer change in wavelength in the SH autocorrelated signal, by measuring the shift in pixels of the FROG trace profile, we were able to determine the correspondence between a pixel and a nanometer.

$$\Delta p = 17 \text{ pixels corresponds to } \Delta\lambda = 1nm$$

$$(28) \quad \Rightarrow \quad \boxed{17 \text{ pixels} = 1 \text{ nm}}$$

The calibration relations between pixels, time, and space (i.e., equations (27) and (28)) are rigorous. This is due to the fact that the divergence of the beam from the BBO crystal to the camera affects the profile of the beam, but it does not affect the shift of the profile due to the induced time delay or change in frequency. Thus, barring some geometrical corrections due to the expansion of the beam as it propagates through the FROG, this project has been essentially completed.

To analyze the expansion of the beam from the crystal to the camera, it important to investigate the effect that dispersion has on the beam profile. In the frequency dimension, The FROG trace showed the grating diffracted autocorrelated light in second order (m = 2). Assuming an incidence angle, α, of $0°$ and an $\lambda ir = 796$ nanometers and using the appropriate sign conventions (see diagram 5), the angle of diffraction, β, was determined from the grating equation.

(29) $m\lambda = d \, (\sin(\alpha) + \sin(\beta))$

$\Rightarrow$ $\dfrac{m\lambda}{d} = \sin(\beta); \{ \beta' = -\beta \}$

$\Rightarrow$ $\boxed{\dfrac{m\lambda}{d} = \sin(\beta')}$

(30)

From equation (30), the angle of diffraction was calculated to be $65°$ (see table 4).

Spectral Enhancement Factor Calculation, F.

Note that the divergence of the blue light (SH) is equal along the time and wavelength dimensions upstream of the diffraction grating. Beyond the grating, an incremental divergence component is added in the wavelength dimension, δ, due to diffraction. Thus, the total enhancement factor, F, is

(31) $F \equiv \Lambda + \delta.$

As described, in the wavelength dimension one pixel represents 0.059 nm of bandwidth (i.e. 17 pixels represents 1 nm of second harmonic light). Since the wavelength calibration made use of fiber optic infrared spectrometer, we know the second harmonic FWHM bandwidth to be 1.45 nm (the measured infrared bandwidth is 2.90 nm). This would amount to a FWHM of 25 pixels without beam size and divergence effects. A spectral bandwidth measurement, which includes δ and Λ, yields 201 pixels,

16

which is eight times larger than the known bandwidth would predict. Thus, the spectral enhancement factor F = 8 (i.e., F = (201 pixels)$_{\text{with A} + \delta}$/ (25 pixels)$_{\text{with F} = 0}$ = 8), which exceeds the time delay enhancement factor, Λ. This enhancement factor is needed to correctly determine pulse spectral and duration from FWHM values.

Time Delay Enhancement Factor Calculation, Λ.

The diffractive component of divergence, δ, can be estimated in the following way. Assume $\delta = 0$. Then, a circular blue beam profile incident on the grating becomes elliptical where the ratio of the semiminor (time) to the semimajor (wavelength) axis is determined from the anamorphic magnification relation set by angles of incidence and diffraction. i.e.,

(32) $\cos (\beta') / \cos (\alpha) = b / a$

see diagram 6). Recalled, β' was calculated to be 65°. In this project an angle of incidence of 0° was used. Thus, equation (32) yields

$$\cos (\beta') / \cos (\alpha) = 0.42. \longrightarrow \text{Anamorphic magnification Effect!}$$

The extent to which this ellipticity of the FROG trace is not 0.42, provides a measure of the incremental divergence attributed alone to grating diffraction, δ, of a blue beam with nonzero bandwidth. The average measured ellipticity of the FROG trace was one. Therefore, $\delta = 1/(0.42) = 2.38$. The temporal scale enhancement factor, Λ, is therefore from equation (31) $\Lambda = 8.0 - 2.38 = 5.62$. This factor is then used for determining the pulse duration (FWHM). In the time dimension a further multiplicatve correction must be added due to an assumed temporal pulse profile. For the Gaussian case, this factor is

0.71 (the inverse of the square root of two). For a different profile such as $sech^2$ the factor is 0.65.

Therefore if the temporal and wavelength FWHM values of a FROG trace are both 200 pixels then the bandwidth is 1.45 nm and the duration is 251 femtoseconds. In this example the time bandwidth product of a single ir pulse ($\Delta v \cdot \Delta t$) ≈ 0.4, which is within ten percent of the theoretical time bandwidth product for a Gaussian and $sech^2$ pulse profile. This is consistent with a transform limited pulse. The data of this project can be linearly scaled from this simple example based on the FWHM data taken on from the FROG trace.

Acknowledgements

References

Acampora, A. Last Mile by Laser. <u>Scientific American</u>. July 2002.

<u>Diffraction Grating Handbook</u>. New York: Milton Roy Company.

Hopkins, J. M. & Sibbet, W. Ultrashort-Pulse Lasers: Big Payoffs in a Flash. <u>Scientific American</u>. September 2000.

Kane, J. D., & Trebino, R (1993). Single-shot Measurement of the Intensity and Phase of an Arbitrary Ultrashort Pulse by Using Frequency-Resolved Optical Gating. <u>Optical Society of America</u>. Vol. 18, No. 10, 823-825.

Kane, J. D., & Trebino, R (1994). Comparison of Ultrashort-Pulse Frequency-Resolved-Optical-Gating Traces for hree Common Beam Geometries. <u>Optical Society of America</u>. Vol 11, No. 11, 1595-1608.

Saleh B. E. A., & Teich C. M (1991). <u>Fundamentals of Photonics</u>. New York: Wiley-interscience.

Salin, F., Georges, P., Roger, G., & Brun, A. Singe-shot measurement of a 52-fs pulse. <u>Applied Optics</u>. Vol 26, No. 21, 4528-4531.

Verdeyen, T. J (1995). <u>Laser Electronics</u>. (Third ed). New Jersey: Prentice Hall Series in Solid State Physical Electronics.

<u>Operator's Manual The Coherent MIRA Model 900-F Laser</u>. California: Coherent Laser Group.
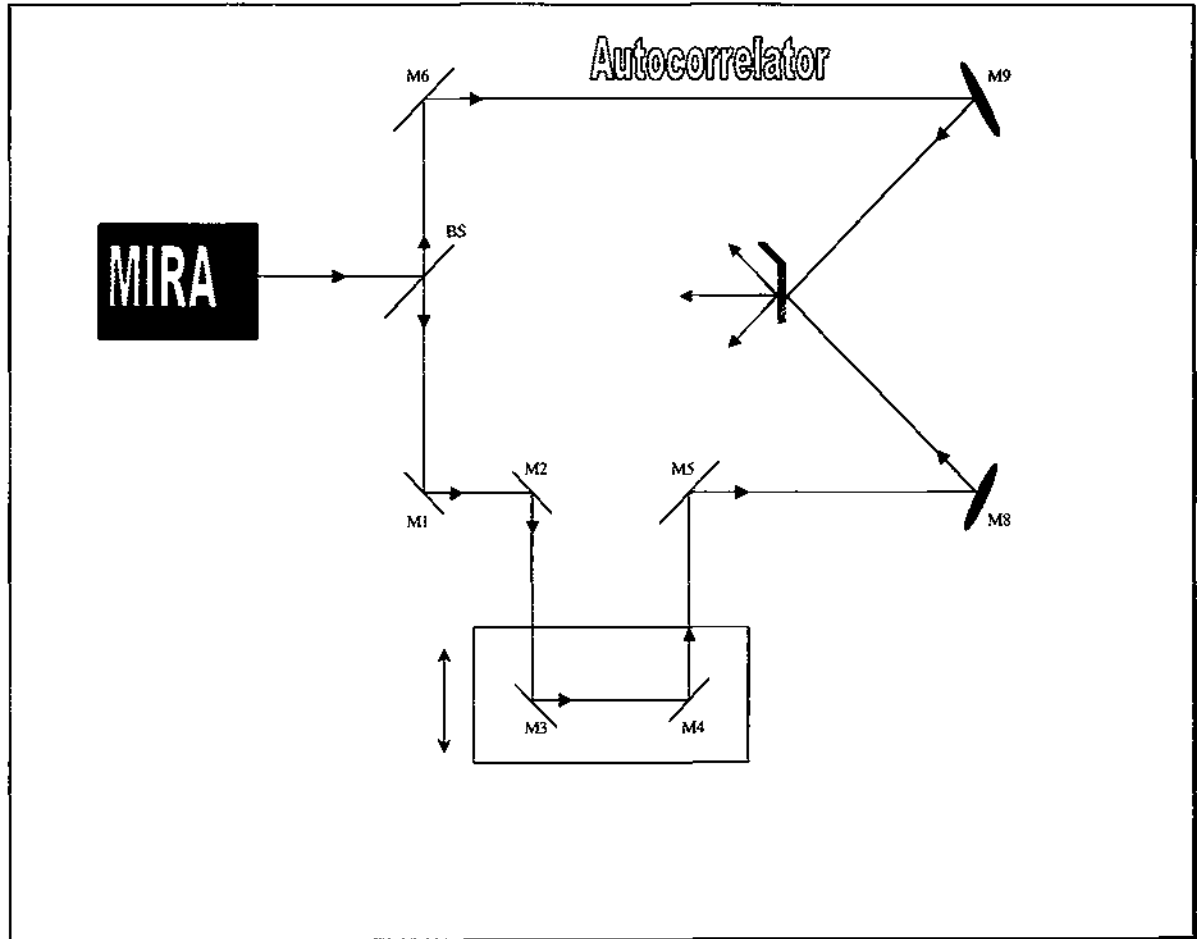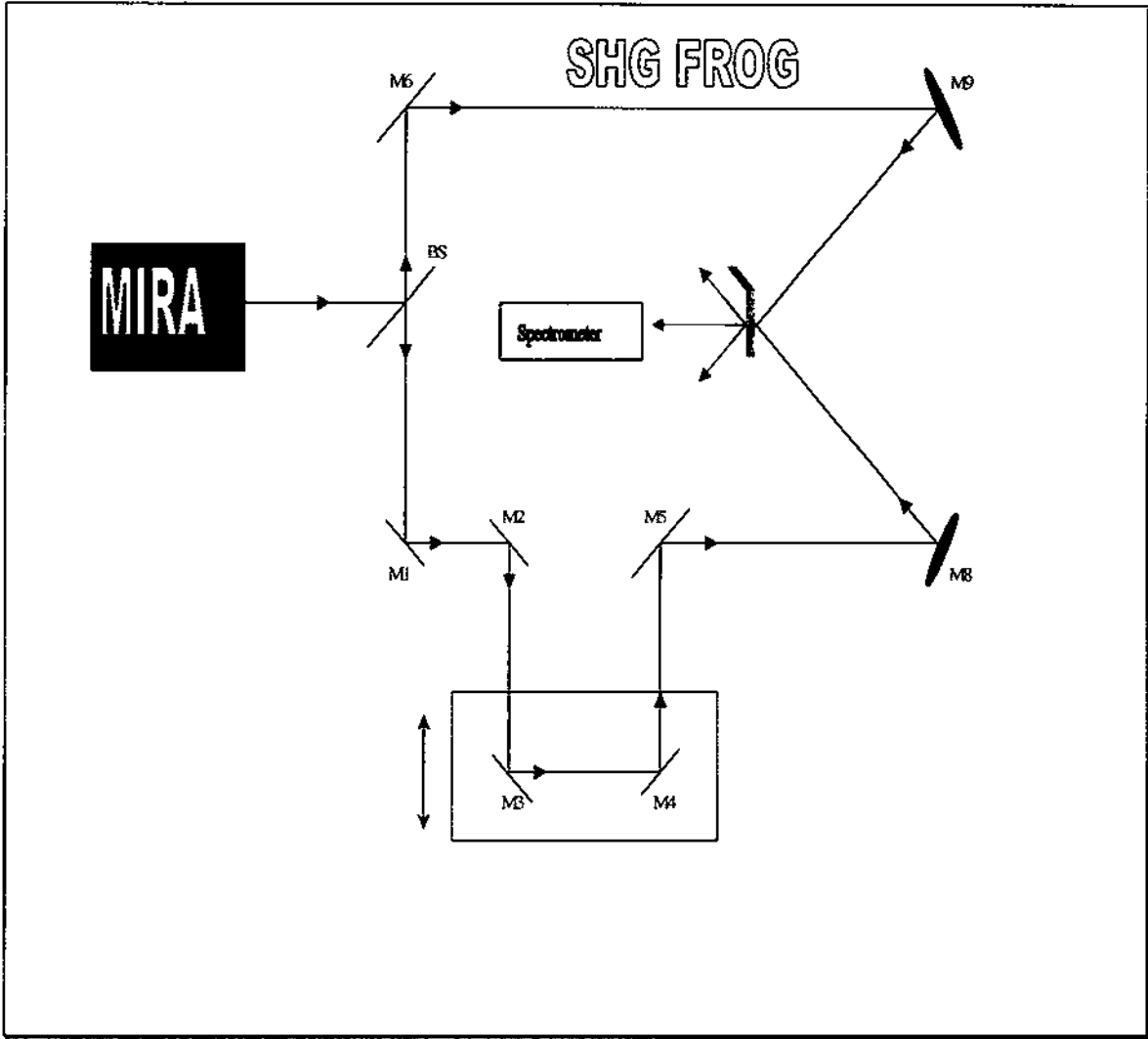
Diagrams

Diagram 1. Autocorrelator optical layout

Diagram 2. SHG FROG optical layout

SHG FROG Pulse Duration Layout Diagram
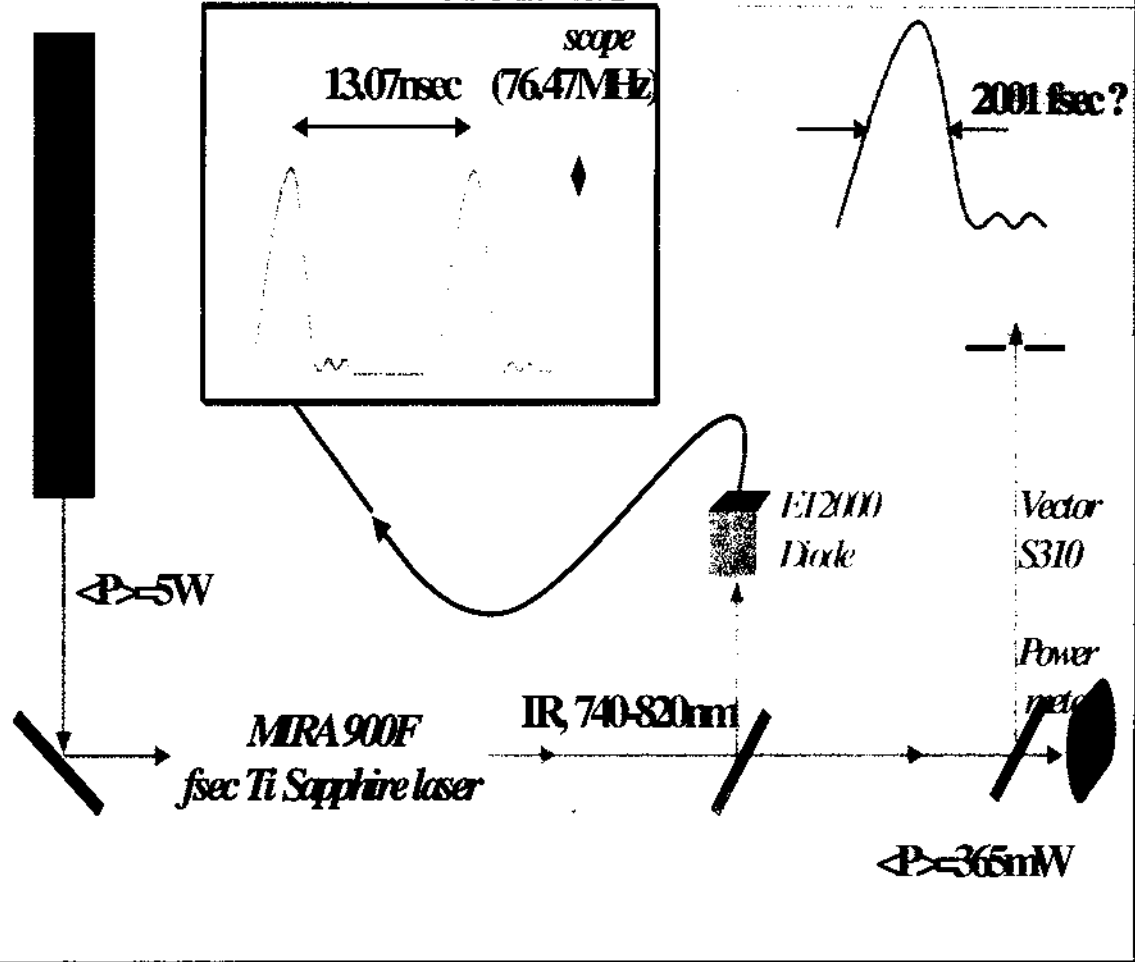
Millennia pump and Ti Sapphire laser

Tektronix 2467B

scope (76.47MHz)

13.07nsec

2001 fsec?

<P>=5W

ET2000
Diode

Vector
S310

Power
meter

MIRA 900F
fsec Ti Sapphire laser

IR, 740-820nm

<P>=365mW

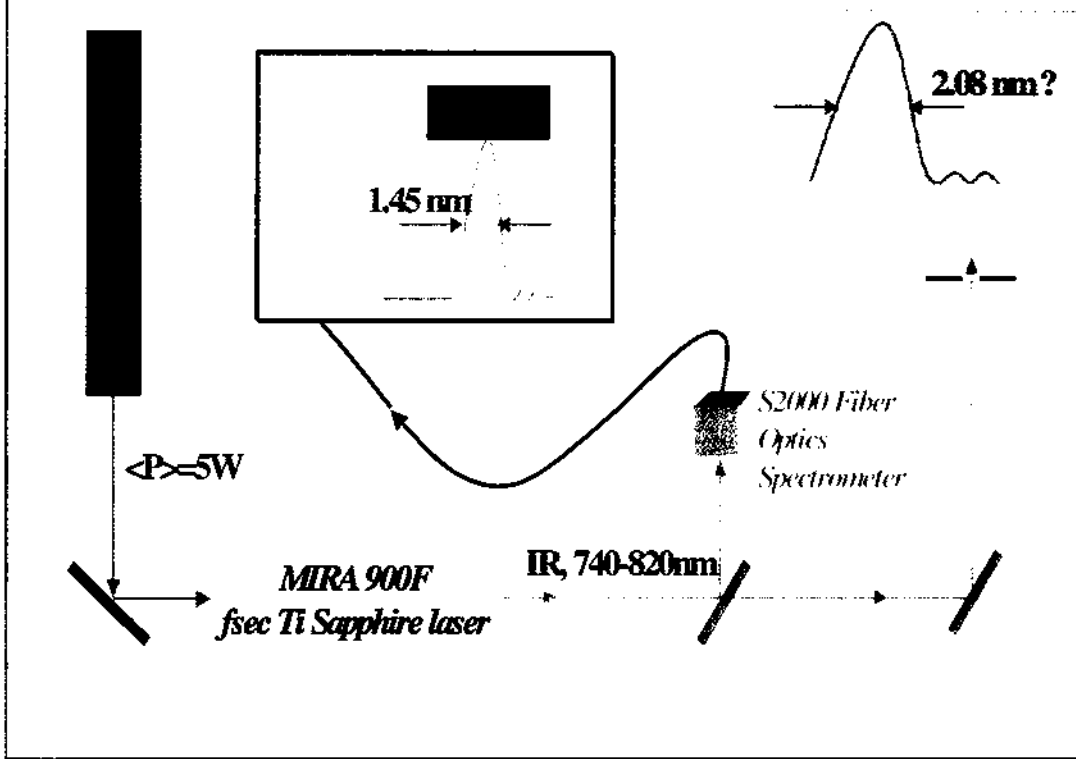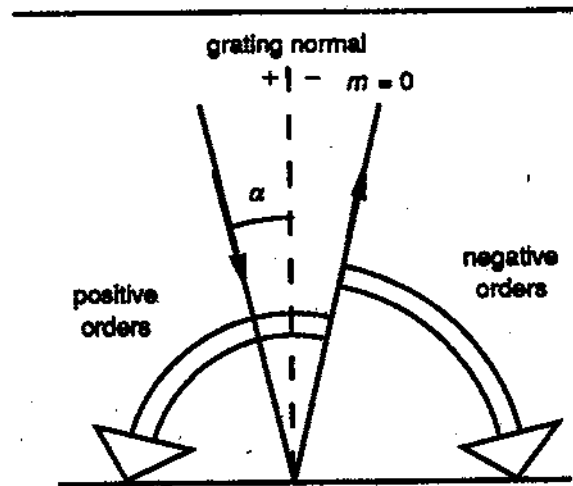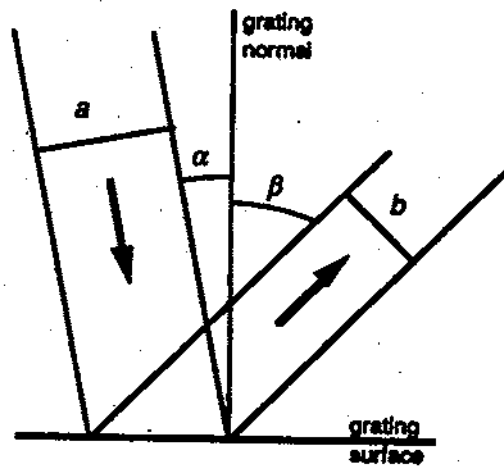**Diagram 3**

SHG FROG Spectral Bandwidth Layout Diagram

Diagram 4

Diagram 5. Sign Convention for the spectral order m.
Source. Diffraction Granting Handbook

Diagram 6. Anamorphic Magnification. The ratio of the beam widths b/a equal the anamorphic magnification
Source. Diffraction Grating Handbook

Tables

WINDOW SIZE: 70-475, 440-470		
Image	FWHM of Profile in Time Axis (Pixels)	Pixel Value at Peak (Pixels)
jv11,610frog80502	205	237.5
jv11,630frog80502	190	236
jv11,650frog80502	206	257
jv11,670frog80502	206	274
jv11,690frog80502	194	285
	Ave. FWHM = 200.2	

Table 1. Time Scale Calibration Data

WINDOW SIZE: 70-475, 440-470			
Optimum Setting at 11.650 mm.			
Image	Time Delay $(\Delta t_0 = \Delta x_0 / c)$ Δx_0 $\qquad$ Δt_0	Pixel value at Peak	Peak Pixel Difference
jv11,610frog80502	-0.040 mm ; -267 fs	237.5	257 − 237.5 = 19.5
jv11,630frog80502	-0.020 mm ; -133 fs	236	257 − 236 = 21
jv11,650frog80502	0	257	257 − 257 = 0
jv11,670frog80502	+0.020 mm ; +133 fs	274	257 − 274 = -17
jv11,690frog80502	+0.040 mm ; 267 fs	285	257 − 285 = -28

Table 2. Autocorrelation Data used for plotting Graph 1. (Note that Optimum Setting Time Delay was defined to be 0)
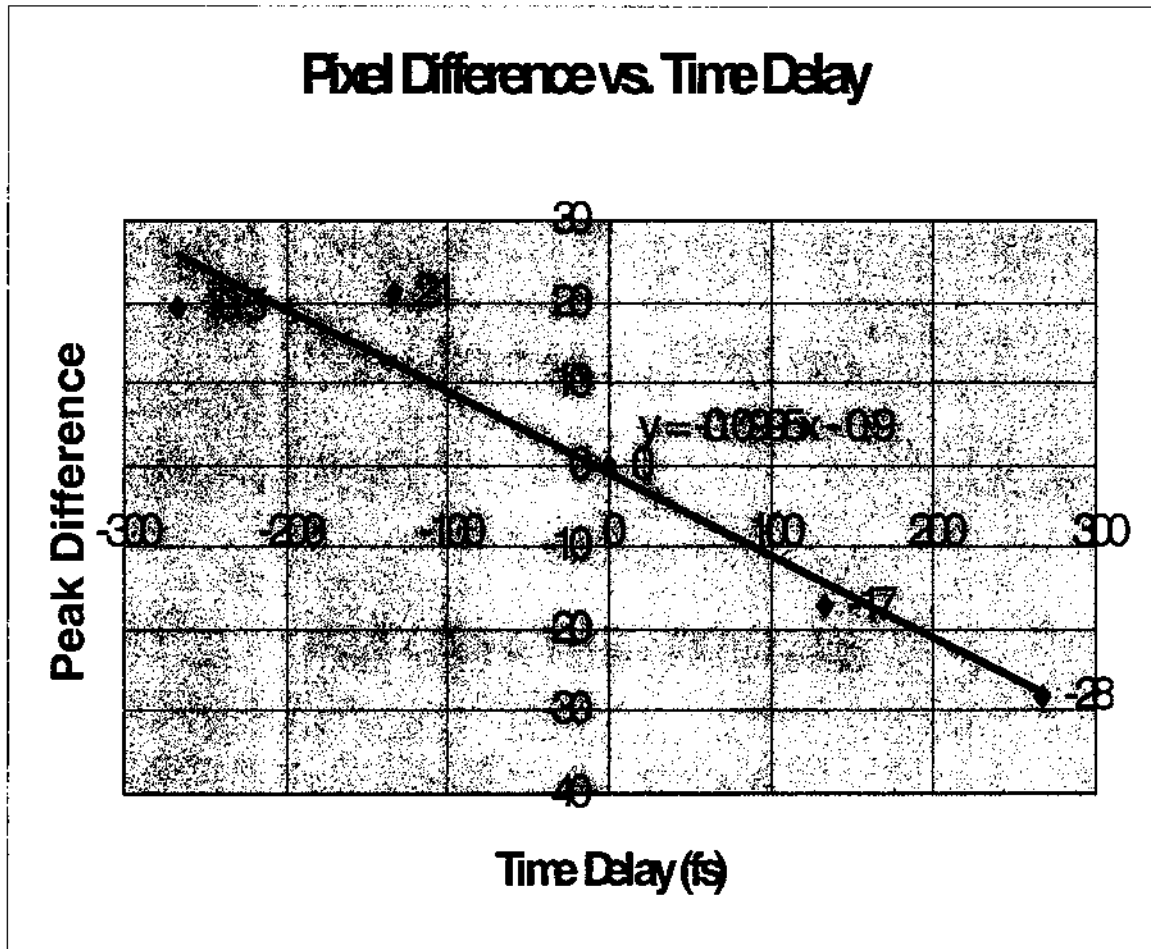
Image	FWHM of Profile in frequency Axis (pixels)	Pixel Value of Peak Frequency	FWHM (S2000)
jv11,660Aug0902frogfreqcal	208	275	1.45 nm
jv11,660Aug0902frogfreqcal#2	194	292	1.35 nm

Table 3. Frequency Scale Calibration Data. (Note a profile shift in frequency axis of 292 − 275 = 17 pixels)

λ (nm)	2·λ/d	β' (°)
375	0.9	64.1
376	0.902	64.5
377	0.905	64.8
378	0.907	65.12
379	0.91	65.45
380	0.912	65.78

Table 4. Computation of Diffraction Angle

Graphs

Graph 1. Δp vs. Δt₀